High-Pressure NMR Spectroscopy

Deutsche Ausgabe: DOI: 10.1002/ange.201505416
Internationale Ausgabe: DOI: 10.1002/anie.201505416

The Energetics of a Three-State Protein Folding System Probed by High-Pressure Relaxation Dispersion NMR Spectroscopy

Vitali Tugarinov, David S. Libich, Virginia Meyer, Julien Roche, and G. Marius Clore**

Abstract: *The energetic and volumetric properties of a three-state protein folding system, comprising a metastable triple mutant of the Fyn SH3 domain, have been investigated using pressure-dependent ^{15}N-relaxation dispersion NMR from 1 to 2500 bar. Changes in partial molar volumes (ΔV) and isothermal compressibilities ($\Delta\kappa_T$) between all the states along the folding pathway have been determined to reasonable accuracy. The partial volume and isothermal compressibility of the folded state are 100 mL mol^{-1} and 40 μL mol^{-1} bar^{-1}, respectively, higher than those of the unfolded ensemble. Of particular interest are the findings related to the energetic and volumetric properties of the on-pathway folding intermediate. While the latter is energetically close to the unfolded state, its volumetric properties are similar to those of the folded protein. The compressibility of the intermediate is larger than that of the folded state reflecting the less rigid nature of the former relative to the latter.*

Pressure, like temperature, constitutes a fundamental thermodynamic variable that can be used to modulate the free-energy landscape of proteins, thereby providing a probe to study conformational fluctuations and folding events.[1] To date, high-pressure protein NMR spectroscopy has largely been confined to examining equilibrium properties[2] and hydrogen/deuterium exchange,[3] as well as slow conformational transitions (on the order of minutes to hours) subsequent to the application of a pressure jump.[4] Two studies have made use of pressure variation and relaxation dispersion to analyze the kinetics of the folding pathways of several metastable proteins.[5,6] The latter studies, however, were confined to a narrow range of pressures extending up to only 120 bar in one case[5] and 250 bar in the other.[6] While relaxation dispersion experiments are sensitive to small changes in rate constants, the changes observed over this narrow pressure range are too small to fully probe the effects of pressure on kinetic parameters and reliably analyze higher-order effects such as compressibility.

To gain detailed insight into the energetic and volumetric properties of a multi-step folding pathway we have carried out ^{15}N Carr–Purcell–Meiboom–Gill (CPMG) relaxation dispersion experiments[7] on a metastable variant of the Fyn SH3 domain[8] over a wide range of pressures from 1 to 2500 bar (0.1 to 250 MPa). The Fyn SH3 variant employed contains three destabilizing mutations, A39V, N53P, V55L (referred to hereafter as Fyn SH3-VPL), and has been shown to fold by a three-state pathway involving rapid exchange between the major folded species **F**, a folding intermediate **I** and the unfolded state **U**.[8a] At 35 °C, the temperature used herein, the populations of **I** and **U** at atmospheric pressure are 2 and 0.7 %, respectively.[8a] The structure of the **I** state has been solved based on backbone chemical shifts and residual dipolar couplings derived from the relaxation dispersion data and reveals partial unfolding at the N and C termini, thereby exposing the side chains of Phe4 and Ala56 and increasing the size of a surface hydrophobic patch relative to the folded state.[8b]

Figure 1 A shows an overlay of a region of the ^{1}H–^{15}N correlation spectrum of U-[^{15}N]-labeled Fyn SH3-VPL acquired at six different pressures ranging from 1 to 2500 bar. Significant changes in $^{1}H_N/^{15}N$ chemical shifts of the folded state **F** are observed as a function of pressure for the majority of residues. Substantial effects of pressure are also evident in the ^{15}N CPMG relaxation dispersion profiles, as illustrated, for example, by the data for L55 and Y10 shown in Figure 1 B and 1 C, respectively, where increasing pressure results in larger dispersion for the former but smaller for the latter. This is a direct consequence of the interplay between the differences in chemical shifts between the various states ($\Delta\omega$) and the rates of exchange between them (k). Qualitatively, as all the interconversion rates between **F**, **I**, and **U** decrease as the pressure is increased, residues with larger $\Delta\omega$ values (e.g. L55) are driven to the slower exchange regime ($k < \Delta\omega$) leading to a reduced relaxation dispersion, while residues with smaller $\Delta\omega$ values (e.g. Y10) are driven closer to the intermediate exchange regime ($k \approx \Delta\omega$) resulting in larger relaxation dispersion.

The pressure dependence of the interconversion rate constants k_{nm}, pertinent to the three-state folding/unfolding pathway shown in Figure 2 A, follows the relationship given in Equation (1),[3,5,9]

$$k_{nm} = (k_B \kappa T/h)\exp(-\Delta G_{TS_{nm}-n}(P)/RT) \quad (1)$$

where the difference in free energy $\Delta G_{TS_{nm}-n}(P)$ between the transition states connecting states m and n (TS_{nm}) and state n as a function of the pressure P is given by Equation (2).

$$\Delta G_{TS_{nm}-n}(P) = \Delta G^0_{TS_{nm}-n} + \Delta V_{TS_{nm}-n}(P - P_0) - \frac{1}{2}\Delta\kappa_{T,TS_{nm}-n}(P - P_0)^2 \quad (2)$$

[*] Dr. V. Tugarinov, Dr. D. S. Libich, Dr. V. Meyer, Dr. J. Roche, Dr. G. M. Clore
Laboratory of Chemical Physics, Building 5
National Institutes of Diabetes and Digestive and Kidney Diseases
National Institutes of Health, Bethesda, MD 20892-0520 (USA)
E-mail: vitali.tugarinov@nih.gov
mariusc@mail.nih.gov

Supporting information for this article is available on the WWW under http://dx.doi.org/10.1002/anie.201505416.

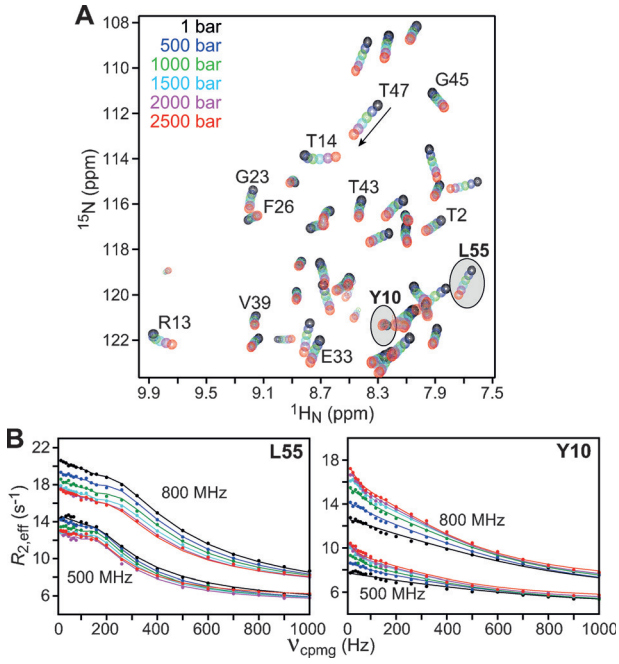

Figure 1. Pressure-dependent NMR of Fyn SH3-VPL. A) ^{1}H-^{15}N correlation spectra acquired at six different pressures ranging from 1 to 2500 bar (800 MHz, 35 °C). The cross-peaks corresponding to the different pressure values are color-coded as indicated on the plot. Selected cross-peaks are labeled. The direction of chemical shift changes with pressure is indicated with an arrow for the peak of T47. B) ^{15}N CPMG relaxation dispersion[7a] profiles for L55 (left) and Y10 (right) acquired at six pressures and two spectrometer fields (500 and 800 MHz) plotted using the same color code as in panel (A). The continuous lines connecting the experimental points represent the results of the global best-fit at all pressures simultaneously to model 2 (see text). Chemical shift differences between states **F** and **I** ($\Delta\omega_{FI}$) and **F** and **U** ($\Delta\omega_{FU}$) for L55 and Y10 are: $\Delta\omega_{FI} = 3.1$ and 2.8 ppm, respectively, and $\Delta\omega_{FU} = 5.4$ and -1.2 ppm, respectively.[8a] Additional examples of ^{15}N CPMG relaxation dispersion fits, and experimental details related to sample preparation and acquisition of the ^{15}N CPMG relaxation dispersion data (that measure the effective relaxation rates of in-phase ^{15}N coherences[7a]) are provided in the Supporting Information.

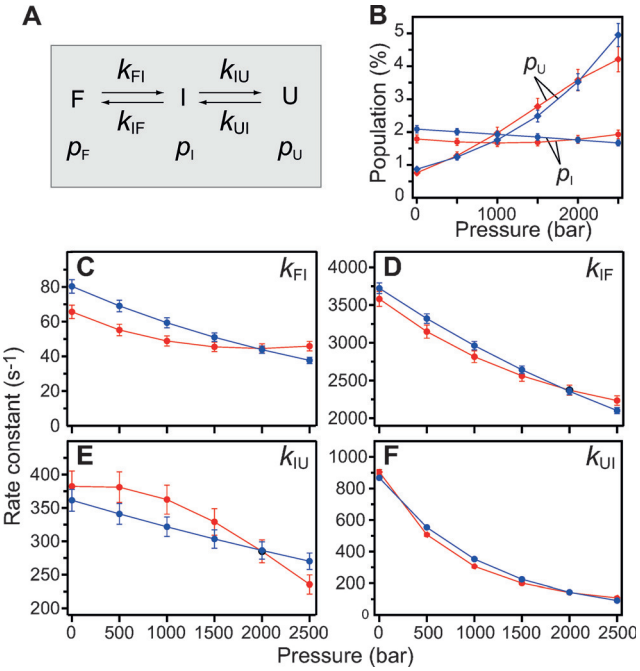

Figure 2. Pressure dependence of folding/unfolding kinetics of Fyn SH3-VPL. A) Three-state model of protein (un)folding used for all the fits to the relaxation dispersion data herein. k_{nm} are the interconversion rate constants and p_n the population of each state. B) Change of p_I and p_U (%) with pressure. Pressure dependencies of C) k_{FI}, D) k_{IF}, E) k_{IU}, and F) k_{UI} rate constants. In each of the plots (B–F), the blue and red filled-in circles represent the results of the global fit to models 1 ($\Delta\kappa_T = 0$; cf. Eq. [3]) and 2 (cf. Eq. [4]), respectively. The lines connecting the values fitted for each pressure are drawn to guide the eye and do not represent the results of a fit.

The subscripts $n,m \in \{\mathbf{F}, \mathbf{I}, \mathbf{U}\}$; $\Delta G^0_{TS_{nm}-n}$ is the free-energy difference at $P_0 = 1$ bar (0.1 MPa); $\Delta V_{TS_{nm}-n}$ and $\Delta\kappa_{T,TS_{nm}-n}$ are the corresponding changes in partial volume V and isothermal compressibility κ_T (defined as dV/dP); k_B is the Boltzmann constant, h Planck's constant, T the temperature (in Kelvin), R the universal gas constant, and κ the transmission coefficient. A value of $\kappa = 1.6 \times 10^{-7}$ is commonly used for protein folding,[10] corresponding to $(k_B\kappa/h) = 3000\ s^{-1}K^{-1}$.

Global fitting of all relaxation dispersion profiles at all pressures simultaneously to the three-state model shown in Figure 2 A with the pressure dependence of the rate constants governed by Equations (1)–(2) was carried out as described in detail in the Supporting Information. The values of $\Delta V_{TS_{nm}-n}$, $\Delta\kappa_{T,TS_{nm}-n}$, and k^0_{nm} (the rate constants connecting states n and m at 1 bar) obtained from the global best-fits are provided in Table 1. To ensure smooth changes in chemical shift differences as a function of pressure, the values of $\Delta\omega$ between states **F** and **I** ($\Delta\omega_{FI}$) and **F** and **U** ($\Delta\omega_{FU}$) were constrained to a quadratic polynomial function of pressure [see Eq. (S7) in the Supporting Information]. The pressure dependence of the four rate constants in Figure 2 A was modeled using either a simple linear relationship assuming $\Delta\kappa_{T,TS_{nm}-n} = 0$ [referred to hereafter as model 1; Eq. (3)],

$$k_{nm}(P) = k^0_{nm} exp\{-\Delta V_{TS_{nm}-n}(P - P_0)/RT\} \quad (3)$$

or the full quadratic relationship [referred to as model 2; Eq. (4)],

$$k_{nm}(P) = k^0_{nm} exp\left\{\left[-\Delta V_{TS_{nm}-n}(P - P_0) + \frac{1}{2}\Delta\kappa_{T,TS_{nm}-n}(P - P_0)^2\right]/RT\right\} \quad (4)$$

Excellent fits were obtained with $\chi^2 = 1.13$ and 1.09 for models 1 and 2, respectively. Although the small decrease in χ^2 for model 2 relative to model 1 is statistically significant (partial F-test $p < 0.0001$), and the optimized values of $\Delta\kappa_T$ are both well defined by the experimental data and lie within the expected range,[11] we report and compare the results from both fits as there is a significant "cross-talk" in the fits between ΔV and $\Delta\kappa_T$, thereby providing a better appreciation of the range of variability of the optimized parameters depending on the model employed. We also note that very similar results are obtained when the relaxation dispersion

Table 1: Values of rate constants (k), changes in partial volumes (ΔV), and changes in isothermal compressibility ($\Delta\kappa_T$) obtained from the global fit of the Fyn SH3-VPL relaxation dispersion data at six pressures ranging from 1 to 2500 bars (35 °C).[a]

	k_0 [s^{-1}][b] (at 1 bar)	ΔV [mL mol^{-1}]	$\Delta\kappa_T$ [μL mol^{-1} bar^{-1}]
TS_{IF}–**F** (k_{FI})	66 ± 4 (80 ± 4)	43 ± 10 (33 ± 3)	22 ± 7
TS_{IF}–**I** (k_{IF})	3581 ± 100 (3723 ± 21)	30 ± 4 (25 ± 1)	7 ± 3
TS_{UI}–**I** (k_{IU})	382 ± 23 (361 ± 16)	−4 ± 9 (13 ± 3)	−20 ± 7
TS_{UI}–**U** (k_{UI})	904 ± 17 (867 ± 12)	132 ± 3 (97 ± 1)	33 ± 3
F–**U**	–	122 ± 15 (76 ± 5)[c]	38 ± 11[c]
F–**I**	–	−14 ± 18 (−8 ± 6)[c]	−15 ± 14[c]

[a] All data are reported with ±1 standard deviation as obtained from the variance-covariance matrix of the nonlinear fit. The values fitted using the linear model of pressure dependence [i.e., $\Delta\kappa_T = 0$, model 1; cf. Eq. (3)] are listed in parentheses. [b] Note that values of k_{FI}, k_{IF}, k_{IU} and k_{UI}, reported previously by Neudecker et al.[8a] at 35 °C and atmospheric pressure (1 bar) are 51 ± 1.6, 2951 ± 55, 389 ± 9, and 924 ± 15 s^{-1}, respectively, corresponding to p_I and p_U values of 1.69 and 0.71 %, respectively. [c] The values of ΔV and $\Delta\kappa_T$ between **F** and **U**, and **F** and **I**, are calculated from the corresponding fitted values for the transition states (first four rows).

data are fit separately at each pressure (i.e. without constraining the rate constants to a particular pressure dependence model). Simultaneous global fitting of the data at all pressures, however, is more robust and ensures smooth continuity of changes in rate constants and $\Delta\omega$ values as a function of pressure (see the Supporting Information for discussion of the changes in $\Delta\omega_{FI}$ and $\Delta\omega_{FU}$ as a function of pressure).

The pressure dependence of the species populations and rate constants are shown in Figure 2B and 2C–F, respectively. The primary effect of pressure is to increase the population (p_U) of the unfolded state **U** from 0.7 % at 1 bar to 5 % at 2500 bar; the population (p_I) of the folding intermediate **I** is virtually pressure-independent (Figure 2B). This is a direct consequence of the differential effects of pressure on the interconversion rate constants between the various states. While k_{FI} and k_{IF} decrease in concert by less than two-fold from 1 to 2500 bar (Figure 2C and D, respectively), k_{IU} (Figure 2E) and k_{UI} (Figure 2F) are affected very differently by pressure, with by far the largest effect exerted on k_{UI} which decreases by almost an order of magnitude from 1 to 2500 bar. These observations are valid irrespective of whether model 1 or 2 is used in the fit, even though significant deviations from exponentiality are seen for the pressure dependence of k_{FI} and k_{IU} using model 2 (red symbols in Figure 2C and E).

The changes in partial molar volumes and isothermal compressibilities obtained from the global fits are referenced to the unfolded state **U** in Figure 3A and B, respectively. Not surprisingly, the volume and compressibility of the folded state **F** are higher than those of the unfolded state **U** by 100 mL mol^{-1} and 40 μL mol^{-1} bar^{-1}, respectively. The largest volume change occurs between state **U** and the transition state TS_{UI} between states **I** and **U**. As expected from the close similarity in the structures of **F** and **I**,[8b] the volume of **I** is close to that of **F** irrespective of the model employed, with V_I larger than V_F by only 8 and 14 mL mol^{-1} for models 1 and 2, respectively (Figure 3A; Table 1). As the differences between the structures of **F** and **I** are minor,[8b] it is conceivable that the somewhat higher partial volumes of **I** result primarily from changes in hydration occuring upon partial unfolding of the N and C termini. Of note, the compressibility of **I** is also higher than that of **F** (Figure 3B; Table 1)—likely a consequence of the presence of some non-native interactions and solvent exposure of hydrophobic side-chains in **I**.

The pressure dependence of the activation free energies $\Delta G_{TS_{nm}-n}$ is shown in Figure 4A. All the values of $\Delta G_{TS_{nm}-n}$ increase with pressure irrespective of the fitting model, with the largest free-energy change occuring between **U** and the corresponding transition state TS_{UI} (compare the pressure dependence of k_{UI} shown in Figure 2F).

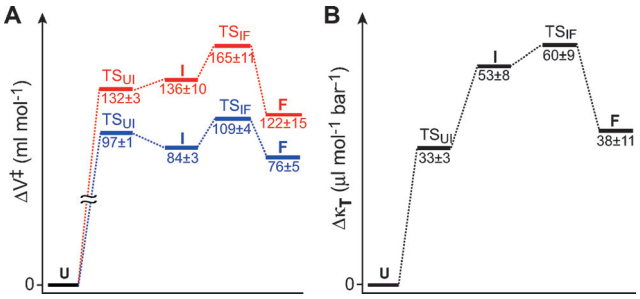

Figure 3. Partial volumes and isothermal compressibilities for the Fyn SH3-VPL three-state protein folding system. A) Partial molar volumes of the Fyn SH3-VPL system referenced to the volume of the unfolded state ($V_U = 0$) obtained from global fitting of the relaxation dispersion data at all pressures to either model 1 [blue; $\Delta\kappa_T = 0$; cf. Eq. (3)] or model 2 [red; cf. Eq. (4)]. B) Isothermal compressibilities referenced to the compressibility of the unfolded state ($\kappa_{T,U} = 0$). The values of the partial volumes and compressibilities of each equilibrium (**F**, **I**, and **U**) and transition state (TS) are indicated below the solid horizontal bars.

The differences in free energies between states m and n, ΔG_{m-n} ($n,m \in \{\mathbf{F}, \mathbf{I}, \mathbf{U}\}$), at each pressure can be calculated from the corresponding equilibrium constants K_{nm} ($= k_{nm}/k_{mn}$) as shown in Equation (5).

$$\Delta G_{m-n} = -RT\ln K_{nm} \quad (5)$$

The pressure dependence of the ΔG values between the **F**, **I**, and **U** states is shown in Figure 4B. The free energy of **I** is close to that of **U** and becomes equi-energetic with the latter at a pressure of 1000 bar (the intersection of ΔG_{I-F} and ΔG_{U-F} in Figure 4B) when states **U** and **I** are equally populated (compare Figure 2B). This implies an approximately equal destabilization of states **I** and **F** by pressure, while the unfolded state **U** remains largely unaffected (see inset in Figure 4B).

To the best of our knowledge, the kinetics of only one other three-state protein folding system as a function of pressure has been investigated to date. In the pressure-dependent relaxation dispersion study of the G48M mutant of

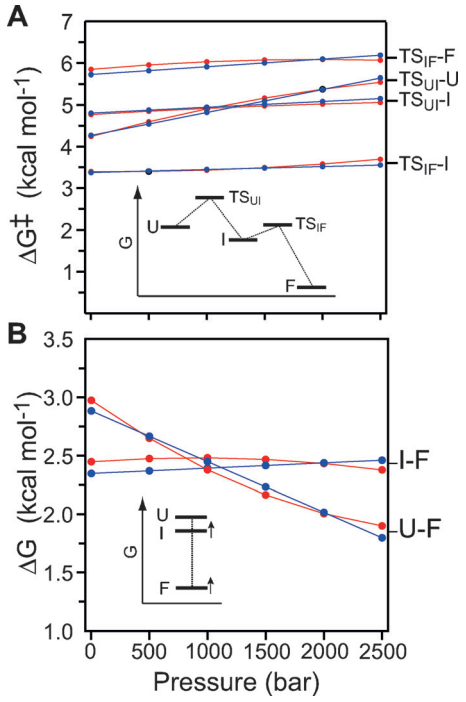

Figure 4. Pressure dependence of activation free energies and free energies for the Fyn SH3-VPL three-state protein folding system. A) Activation free energies [Eq. (2)] and B) free-energy differences [Eq. (5)] between the states derived from the results of the global fit of the relaxation dispersion data at all pressures to either model 1 [$\Delta\kappa_T = 0$; blue circles; cf. Eq. (3)] or model 2 [red circles; cf. Eq. (4)]. Note that $\Delta G_{U-F} = \Delta G_{I-F} + \Delta G_{U-I}$. Free-energy level diagrams of the three-state folding equilibrium are shown in the insets of both panels. The arrows in the inset of panel (B) indicate the direction of the free-energy changes of states **F** and **I** with pressure.

the Fyn SH3 domain, Kay and co-workers used a narrow range of pressures from 1 to 120 bar to derive the volumetric properties of the system using the linear model of pressure dependence (i.e. $\Delta\kappa_T = 0$).[5] Although the reported volume change, ΔV_{F-U} between the states **F** and **U** of 70 ± 3 mL mol^{-1} is comparable to that found here for Fyn SH3-VPL, some important differences emerge in relation to the volume of the intermediate state **I**. In particular, in the G48M mutant, the volume of the **I** state lies in between those of **U** and **F**,[5] while in Fyn SH3-VPL (at 35 °C) the volume of **I** is slightly higher than that of **F** irrespective of the fitting model employed (Figure 3 A), indicating differences in structure and/or hydration between the folding intermediates of the Fyn SH3-G48M and VPL mutants. In addition, the much wider range of pressures (1 to 2500 bar) used herein permits reliable estimates of $\Delta\kappa_T$ for all the states on the Fyn SH3-VPL folding pathway (Figure 3 B). Notably, the positive values of $\Delta\kappa_{T,F-U}$ obtained for Fyn SH3-VPL (Table 1) are consistent with expectations based on prior relaxation dispersion and volumetric measurements,[6] as well as theoretical predictions.[11a]

In summary, we have used ^{15}N CPMG relaxation dispersion NMR spectroscopy to measure the pressure-dependent folding/unfolding kinetics of a triple metastable mutant of the Fyn SH3 domain, which is known to fold through a sparsely populated on-pathway intermediate.[8] The exquisite sensitivity of NMR relaxation dispersion to even small changes in rate constants and the wide range of pressures used (up to 2500 bar) enabled us to reliably quantify the changes in partial molar volumes and isothermal compressibilities along the folding trajectory. The insights gained into the energetic and volumetric properties of the on-pathway intermediate are of particular interest: while the intermediate state is energetically close to the unfolded state, its volumetric properties are similar to those of the native folded protein. Further, the compressibility of the intermediate state is larger than that of the folded state, indicating the structure of the intermediate is less rigid than that of the folded state. Pressure-dependent relaxation-based NMR methods represent a powerful complement to conventional approaches for measuring volumetric and energetic properties associated with protein folding where pH, denaturants or temperature are used to perturb the folding equilibria—all the more so in cases of complex, multistep folding pathways.

Acknowledgements

This work was supported by the Intramural Program of NIDDK, NIH and by the AIDS Targeted Antiviral Program of the Office of the Director of the NIH (to G.M.C.).

Keywords: high-pressure NMR spectroscopy · kinetics · protein folding · proteins · relaxation dispersion

How to cite: *Angew. Chem. Int. Ed.* **2015**, *54*, 11157–11161
Angew. Chem. **2015**, *127*, 11309–11313

[1] a) J. Jonas, *Science* **1982**, *216*, 1179–1184; b) K. Akasaka, *Chem. Rev.* **2006**, *106*, 1814–1835; c) K. Akasaka, R. Kitahara, Y. O. Kamatari, *Arch. Biochem. Biophys.* **2013**, *531*, 110–115; d) F. Hirata, K. Akasaka, *J. Chem. Phys.* **2015**, *142*, 044110; e) G. A. P. de Oliveira, J. L. Silva, *Proc. Natl. Acad. Sci. USA* **2015**, *112*, E2775–E2784.

[2] a) J. B. Rouget, T. Aksel, J. Roche, J. L. Saldana, A. E. Garcia, D. Barrick, C. A. Royer, *J. Am. Chem. Soc.* **2011**, *133*, 6020–6027; b) Y. Fu, V. Kasinath, V. R. Moorman, N. V. Nucci, V. J. Hilser, A. J. Wand, *J. Am. Chem. Soc.* **2012**, *134*, 8543–8550; c) J. Roche, J. A. Caro, D. R. Norberto, P. Barthe, C. Roumestand, J. L. Schlessman, A. E. Garcia, B. E. Garcia-Moreno, C. A. Royer, *Proc. Natl. Acad. Sci. USA* **2012**, *109*, 6945–6950; d) N. Vajpai, L. Nisius, M. Wiktor, S. Grzesiek, *Proc. Natl. Acad. Sci. USA* **2013**, *110*, E368–E376; e) H. R. Kalbitzer, I. C. Rosnizeck, C. E. Muente, S. P. Narayanan, V. Kropf, M. Spoener, *Angew. Chem. Int. Ed.* **2013**, *52*, 14242–14246; *Angew. Chem.* **2013**, *125*, 14492–14496; f) M. Beck Erlach, J. Koehler, B. Moeser, D. Horinek, W. Kremer, H. R. Kalbitzer, *J. Phys. Chem. B* **2014**, *118*, 5681–5690.

[3] E. J. Fuentes, A. J. Wand, *Biochemistry* **1998**, *37*, 9877–9883.

[4] a) W. Kremer, M. Arnold, C. E. Munte, R. Hartl, M. B. Erlach, J. Koehler, A. Meier, H. R. Kalbitzer, *J. Am. Chem. Soc.* **2011**, *133*, 13646–13651; b) J. Roche, M. Dellarole, J. A. Caro, D. R. Norberto, A. E. Garcia, B. Garcia-Moreno, C. Roumnestand, C. A. Royer, *J. Am. Chem. Soc.* **2013**, *135*, 14610–14618.

[5] I. Bezsonova, D. M. Korzhnev, R. S. Prosser, J. D. Forman-Kay, L. E. Kay, *Biochemistry* **2006**, *45*, 4711–4719.

[6] D. M. Korzhnev, I. Bezsonova, F. Evanics, N. Taulier, Z. Zhou, Y. Bai, T. V. Chalikian, R. S. Prosser, L. E. Kay, *J. Am. Chem. Soc.* **2006**, *128*, 5262 – 5269.
[7] a) D. F. Hansen, P. Vallurupalli, L. E. Kay, *J. Phys. Chem. B* **2008**, *112*, 5898 – 5904; b) A. G. Palmer 3rd, *J. Magn. Reson.* **2014**, *241*, 3 – 17.
[8] a) P. Neudecker, A. Zarrine-Afsar, W. Y. Choy, D. R. Muhandiram, A. R. Davidson, L. E. Kay, *J. Mol. Biol.* **2006**, *363*, 958 – 976; b) P. Neudecker, P. Robustelli, A. Cavalli, P. Walsh, P. Lundstrom, A. Zarrine-Afsar, S. Sharpe, M. Vendruscolo, L. E. Kay, *Science* **2012**, *336*, 362 – 366.
[9] K. E. Prehoda, E. S. Mooberry, J. L. Markley, *Biochemistry* **1998**, *37*, 5785 – 5790.
[10] S. J. Hagen, J. Hofrichter, A. Szabo, W. A. Eaton, *Proc. Natl. Acad. Sci. USA* **1996**, *93*, 11615 – 11620.
[11] a) N. Taulier, T. V. Chalikian, *Biochim. Biophys. Acta Protein Struct. Mol. Enzymol.* **2002**, *1595*, 48 – 70; b) T. V. Chalikian, *Annu. Rev. Biophys. Biomol. Struct.* **2003**, *32*, 207 – 235; c) J. L. Silva, G. Weber, *Annu. Rev. Phys. Chem.* **1993**, *44*, 89 – 113.

Received: June 12, 2015
Published online: August 4, 2015

